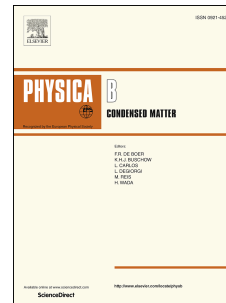


Journal Pre-proof

Remarkable performance optimization of inverted p-i-n architecture perovskite solar cell with CZTS as hole transport material

Syed Zulqarnain Haider, Hafeez Anwar, Mingqing Wang



PII: S0921-4526(21)00444-0

DOI: <https://doi.org/10.1016/j.physb.2021.413270>

Reference: PHYSB 413270

To appear in: *Physica B: Physics of Condensed Matter*

Received Date: 25 February 2021

Revised Date: 8 June 2021

Accepted Date: 12 July 2021

Please cite this article as: S.Z. Haider, H. Anwar, M. Wang, Remarkable performance optimization of inverted p-i-n architecture perovskite solar cell with CZTS as hole transport material, *Physica B: Physics of Condensed Matter* (2021), doi: <https://doi.org/10.1016/j.physb.2021.413270>.

This is a PDF file of an article that has undergone enhancements after acceptance, such as the addition of a cover page and metadata, and formatting for readability, but it is not yet the definitive version of record. This version will undergo additional copyediting, typesetting and review before it is published in its final form, but we are providing this version to give early visibility of the article. Please note that, during the production process, errors may be discovered which could affect the content, and all legal disclaimers that apply to the journal pertain.

© 2021 Published by Elsevier B.V.

Hafeez Anwar: Conceptualization, Methodology, Supervision and Funding acquisition. Syed **Zulqarnain Haider**: Data curation, Software, Visualization, Investigation, Validation, Writing-Original draft preparation. **Mingqing Wang**: Resources, Writing- Reviewing and Editing

Journal Pre-proof

Remarkable Performance Optimization of Inverted p-i-n Architecture Perovskite Solar Cell with CZTS as Hole Transport Material

Syed Zulqarnain Haider¹, Hafeez Anwar¹, * and Mingqing Wang²

¹Department of Physics, University of Agriculture Faisalabad, Pakistan-38040

²Institute for Materials Discovery, University College of London United Kingdom

*Corresponding author's e-mail: hafeez.anwar@gmail.com

Abstract

Hole transport material (HTM) is a major component of perovskite solar cells (PSCs). PEDOT: PSS, an organic HTM, is widely used in inverted (p-i-n) PSCs. While PEDOT: PSS is unstable, expensive and its acidic nature could deteriorate the absorber. Copper zinc tin sulphide (CZTS), an inorganic semiconductor can be used as HTM due to its properties such as low cost, ease of synthesis and high hole mobility. In this work, device simulation of inverted (p-i-n) PSC was performed with CZTS as HTM to exploit its maximum capability. Remarkable power conversion efficiency (PCE) of 25.43 % was achieved after optimizing the performance. Device performance was strongly affected by thickness and electron affinity of HTM as well as diffusion length of carriers. PCE of real fabricated device was also found to be 9.72 %. This work demonstrates CZTS is a promising candidate to replace PEDOT: PSS from both experimental and theoretical perspectives.

Keywords: Device simulation, power conversion efficiency, hole transport material, copper zinc tin sulphide, perovskite solar cell

1. Introduction

Organometal halide perovskite solar cells (PSCs) have attracted attention of researchers owing to their striking characteristics such as solution processability, small binding energy, long diffusion length of charge carriers as well as high absorption co-efficient [1–4]. In 2009, MAPbI₃ and MAPbBr₃ were used as absorbers in PSCs and power conversion efficiency (PCE) of 3.61 % and 3.13 % were achieved respectively [5]. Performance of the PSCs had been optimized by many researchers since 2009 and PCE had been achieved up to 25 % for the last few years [6–8]. Various structures of PSCs had been developed, including mesoporous PSCs [9], planar heterojunction PSCs [10] and perovskite sensitized solar cells [11]. Planar heterojunction is composed of simple structure as compared to mesoporous structure which requires high processing temperature [12]. There are two kinds of planar structured PSCs, normal structure (n-i-p) and inverted structure (p-i-n). The typical architecture of n-i-p PSC is TCO/electron transport material (ETM)/ absorber/HTM/metal. Till now, PCE of more than 20 % have been achieved for n-i-p type PSCs [13,14]. While p-i-n PSCs typically use organic charge transport layers and possess some benefits such as processing at low temperature, less current hysteresis, good stability, high throughput and easy for fabrication for industrial application [15–17]. The typical architecture of p-i-n PSC is TCO/HTM/ absorber/ETM/metal. The mostly used HTM in p-i-n PSCs is PEDOT: PSS owing to high conductivity, better film deposition and high work function [18]. At the same time, PEDOT: PSS also has disadvantages such as acidic and hygroscopic nature which causes degradation and instability of the device as well as corrosion of substrate [19]. Recently, PCE of p-i-n PSCs had been improved from 3.9 % [20] to 18.1 % [21] when PEDOT: PSS was used as HTM, but only 27 % of its initial PCE was retained after 14 days [22]. Moreover, dimethyl sulfoxide (DMSO), lithium bis(trifluoromethanesulfonic)imide (Li-TFSI) and tert-Butylpyridine

(TBP) are employed as dopants to further enhance the conductivity of PEDOT: PSS as HTM. While those dopants are more susceptible to humidity which causes additional stability issues of PSCs in moisture [21,23,24]. Therefore, it is dire need to replace PEDOT: PSS with stable, cost-effective, and efficient HTM in p-i-n PSCs. CZTS is a widely studied p-type semiconductor material in thin film solar cells with adjustable bandgap, high mobility, good stability and low cost [25,26]. Hydrophobic property of CZTS also can protect the absorber from moisture thus enhancing the stability of device [27]. In addition to this, transmission spectrum of CZTS and absorption spectrum of MAPbI_3 are close-matched which provides an opportunity for its application in tandem cells [28–30]. Therefore, CZTS is a promising choice for the replacement of PEDOT: PSS as HTM in p-i-n PSCs in order to enhance the performance and stability of PSCs.

Understanding of various mechanisms in the device. There are many device simulation programs available for theoretical performance investigation of PSCs such as AMPS [31], COMSOL [32], SILVACO [33], WxAMPS[34] and SCAPS[35,36]. Amongst these simulation programs, Solar Cell Capacitance Simulator (SCAPS) was frequently used because of its advantages like ability to simulate PSCs up to seven layers with J-V curve analyses, QE analysis, AC measurements and grading of all materials. It also provides the great convenience of batch calculation, scripting, and recording of solar cell parameters as function of any semiconductor parameter. But there are also certain limitations such as it does not simulate PSCs in time domain and thus transient phenomenon cannot be performed. Furthermore, Solar Cell Capacitance Simulator (SCAPS) was used by many researchers for the simulation of n-i-p PSCs [6–8] while little work was found in literature in terms of device fabrication and performance optimization for p-i-n PSCs with any simulation tool. For example, device modelling of n-i-p type PSC was performed with CZTS as HTM in which eleven parameters were optimized to achieve PCE of 22.7 % [37]. Experimentally, it is very difficult to

optimize such number of parameters in the same device. In this work, PSC with p-i-n architecture is fabricated with CZTS as HTM and PCBM as ETM, with MAPbI₃ being used as absorber. Device simulation is then carried out to optimize the performance of the device. For this purpose, SCAPS is used to study the effect of various physical parameters on the performance of device. Properties of both HTM and MAPbI₃ were optimized, including doping density (N_A), diffusion length, thickness and density of states (N_c) of absorber, along with electron affinity (χ), thickness and doping density (N_A) of HTM. This work provides a guidance for device design and optimization of p-i-n PSCs in terms of experimental and theoretical aspects.

2. Experimental details

2.1 Materials

Copper acetate hydrate (Cu(OAc)₂·H₂O, Sigma Aldrich, 98 %), Tin chloride dihydrate (SnCl₂·2H₂O, Sigma Aldrich, 98 %), Zinc chloride (ZnCl₂, Merck, 99.9 %), Thiourea (Sigma Aldrich, 99 %), hydroiodic acid (Alfa Aesar, 55-58 wt. %), lead iodide (Arcos Organics, 99 %), methylamine (Sigma Aldrich, 40 wt. % in H₂O), Zn powder (median 6-9 μ m, Alfa Aesar 97.5 %), dimethyl sulfoxide (DMSO, Merck, 99.7 %), hydrochloric acid (HCl, Merck, 37 wt. %), Acetone (Merck, 99.5 %), isopropanol (Merck, 99 %), Chlorobenzene (C₆H₅Cl, Merck, 99.8 %), Phenyl-C61-butyric acid methyl ester (PCBM, Merck, 99.5 %) were used without further purification.

2.2 Device fabrication

Zinc powder and HCl were used to etch the fluorine doped tin oxide (FTO) glass. After that, FTO was sequentially washed with isopropanol, deionized water and acetone following ultra-sonication for 15 minutes and air plasma treatment for 10-15 minutes respectively. Clear CZTS precursor solution was prepared by dissolving it into DMSO and then added to a vial containing 4 mM of

(Cu(OAc)₂·H₂O), 2.75 mM of SnCl₂·2H₂O, 2.80 mM of ZnCl₂ and 13.2 mM of thiourea. Spin coating was used to deposit compact layer of CZTS on FTO glass by using CZTS precursor solution. For thermal annealing of CZTS, the deposited film was immediately put into tube furnace and annealed at 550 °C for 30 minutes with 50 g of Sulfur under Ar protection. The atomic ratio of CZTS is Cu: Zn: Sn: S = 20.84: 14.41:11.94: 52.81, for which the ratio of Cu / Zn+Sn=0.79 and the ratio of Zn / Sn=1.21. The MAPbI₃ perovskite solution (1.0 M) was spin coated in one-step at 4000 rpm for 30 seconds. 100 μL of C₆H₅Cl was poured on the spinning substrate for 18 seconds prior to the end of the process. Perovskite film was then annealed at 100 °C for 60 minutes on a hotplate. The ETM layer of 20 mg/ml PCBM in chlorobenzene was deposited by spin-coating at 2000 rpm for 30 seconds. Finally, 120 nm of silver was thermally evaporated on the top of the device at deposition rate of 1 Å/s when pressure becomes smaller than 10⁻⁶ mbar. Device fabrication flow diagram is shown in Fig. 1.

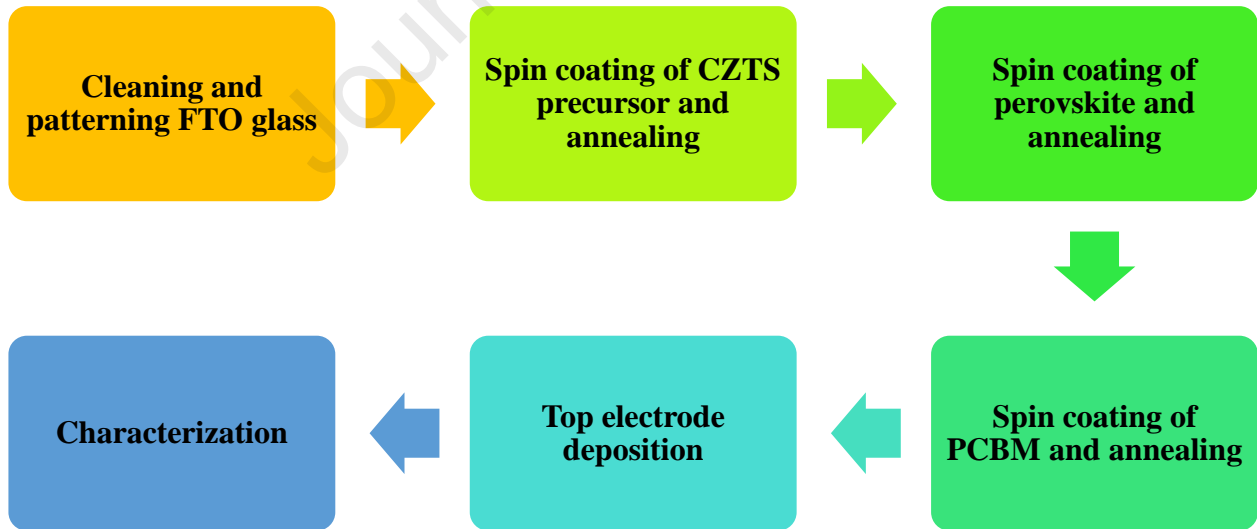


Fig. 1. Device fabrication flow diagram

Source meter unit (Keithley 2400) was used to measure current-voltage characteristics of device under irradiation of 100 mW cm^{-2} with solar simulator (Model 94021A, Oriel Instruments, USA)

3. Device simulation details

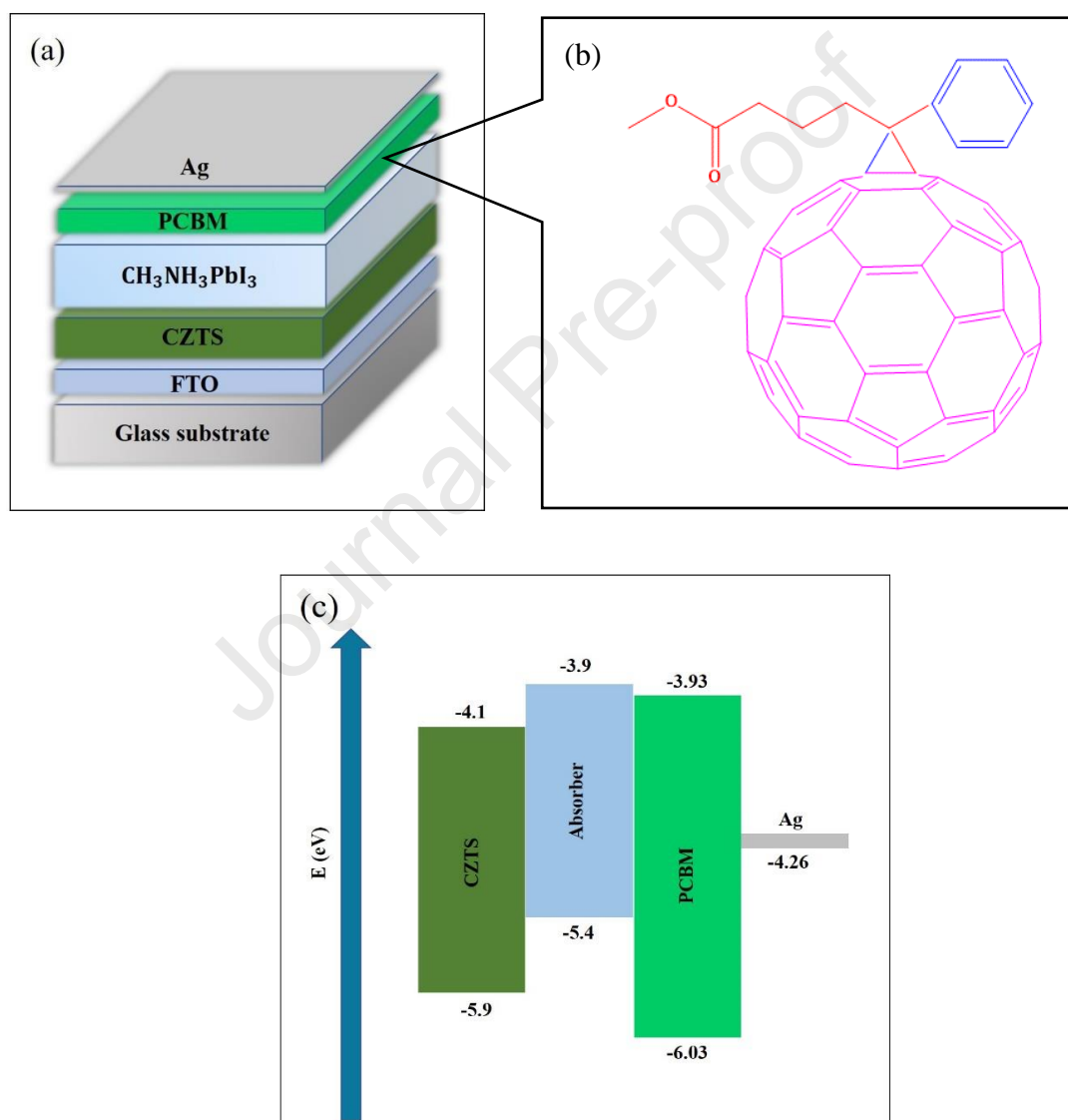


Fig. 2. (a) Schematic diagram of inverted PSC with CZTS as HTM (b) Structural formula of PCBM (c) Band alignment diagram of inverted PSC with CZTS as HTM

The device simulation of p-i-n type PSC is carried out with the device architecture FTO / CZTS / MAPbI₃ / PCBM / Ag as shown in Fig. 2a. FTO is used as front electrode. CZTS is applied as HTM, MAPbI₃ is designated as absorber, PCBM is acted as ETM and Ag is used as back metal contact. Structural formula of PCBM is shown in Fig. 2b and Band alignment diagram is shown in Fig. 2c. Defect density (N_t) can be used to determine the quality of absorber and to calculate diffusion length of electrons (L_n) and holes (L_p) in the absorber. Energetic distribution in absorber is single type with characteristic energy of 0.1 eV and defect energy level lies near valence band edge. Material properties of each layer as well as defect parameters of interfaces are shown in Table 1 and Table 2. Thermal velocities of charge carriers are set to be 10^7 cm^{-1} . The photo reflectance is assumed as zero at interfaces as well as at the surface.

Table 1

Defect parameters of interfaces and absorber of p-i-n type PSC with CZTS as HTM

Parameters	CH ₃ NH ₃ PbI ₃	PCBM/CH ₃ NH ₃ PbI ₃ interface	CH ₃ NH ₃ PbI ₃ /CZTS interface
Defect type	Neutral	Neutral	Neutral
Capture cross section for electrons (cm²)	2×10^{-14}	1×10^{-19}	1×10^{-19}
Capture cross section for holes (cm²)	2×10^{-14}	1×10^{-19}	1×10^{-19}
Energetic distribution	Single	Single	Single
Energy level with respect to E_v (eV)	0.1	0.600	0.600
Characteristic energy (eV)	0.1	0.1	0.1
Total density (cm⁻³)	1×10^{13} to 1×10^{19}	1×10^{10}	1×10^{10}

Table 2

Device simulation parameters of inverted PSC with CZTS as HTM

Parameters	TCO	HTM (CZTS)	Absorber (CH ₃ NH ₃ PbI ₃)	ETM (PCBM)
Thickness (μm)	0.500	0.200	0.250	0.010
Electron affinity χ (eV)	4	4.1 [38]	3.9 [39]	3.93 [40]
Band gap energy E_g (eV)	3.5	1.8 [41]	1.50 [42]	2.1 [43]
Relative permittivity ϵ_r	9	10 [44]	6.5 [45]	3.5 [46]
Effective conduction band density N_c (cm^{-3})	2.0×10^{18}	1×10^{18}	2.2×10^{18} [47]	1.5×10^{19}
Effective valance band density N_v (cm^{-3})	1.8×10^{19}	1.3×10^{19}	1.8×10^{19} [47]	1.0×10^{18}
Electron mobility μ_n ($\text{cm}^2 \text{V}^{-1} \text{s}^{-1}$)	20	1×10^2 [48]	10 [49]	1×10^{-3}
Hole mobility μ_p ($\text{cm}^2 \text{V}^{-1} \text{s}^{-1}$)	8	3×10^1 [50]	10	2×10^{-4} [51]
Donor concentration N_D (cm^{-3})	2.0×10^{19}	0	0	4×10^{15}
Acceptor concentration N_A (cm^{-3})	0	1×10^{17}	5×10^{16}	0
Defect density N_t (cm^{-3})	1×10^{15}	1×10^{17}	1×10^{16}	1×10^{14}

4. Results and discussion

Cross-section SEM image (Fig. 3a) of the prepared device shows the thickness of the whole device is around 700 nm. The bottom layer is composed of CZTS layer and the top layer is composed of thicker MAPbI₃ absorber layer. The PCBM layer is very thin and cannot be seen very clearly. Between CZTS and MAPbI₃ layer, a few pin holes can be seen, which is due to the hydrophobic property of CZTS surface. Optimization of UV-O₃ treatment time of CZTS could optimize the wetting properties of MAPbI₃ solution with CZTS surface. From XRD characterization in Fig. 3b, it is observed that the characteristic peaks of MAPbI₃ appear for the (100), (110), (111), (200),

(210), (221) and (310) lattice planes, corresponding to the 2θ positions of 13.85, 19.62, 24.10, 27.89, 31.29, 42.39 and 44.78°, respectively, which corresponds to cubic crystal structure.

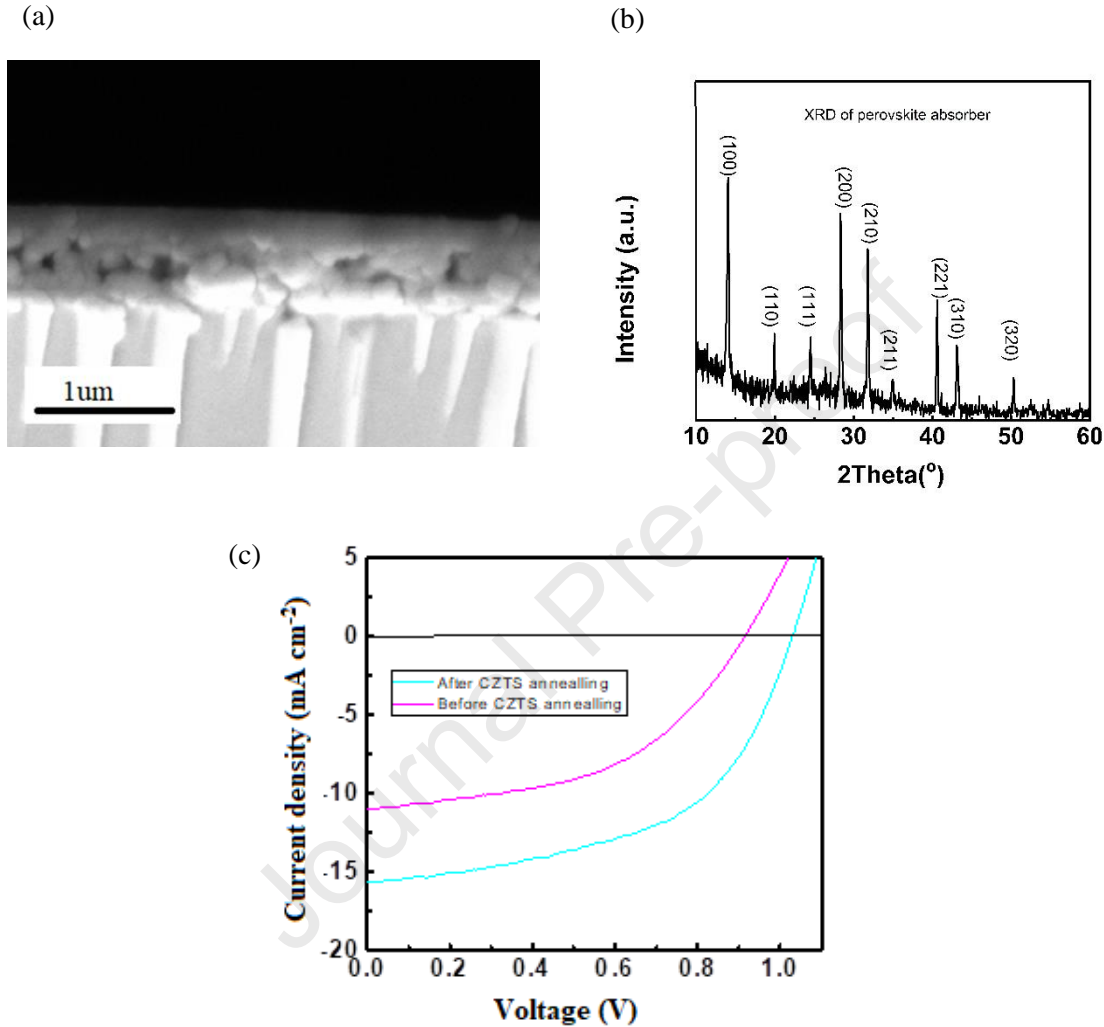


Fig.3. (a) SEM cross section of device (b) XRD of absorber (c) Experimental J-V curves of CZTS based inverted PSC

J-V curves of the fabricated device are shown in Fig. 3c. The performance parameters such as open circuit voltage (V_{oc}) of 1.03 V, fill factor (FF) of 53.24 %, short circuit current density (J_{sc}) of 15.63 mA/cm² and PCE of 9.72 % were obtained after the annealing of CZTS. Theoretical J-V and

QE curves are drawn with the initial parameters given in Table 1 and Table 2 and are shown in curves in Fig. 4. V_{oc} of 1.07 V, FF of 54.85 %, J_{sc} of 16.88 mA/cm^2 and PCE of 9.95 % are obtained, showing consistency with the performance of real inverted PSC with CZTS as HTM.

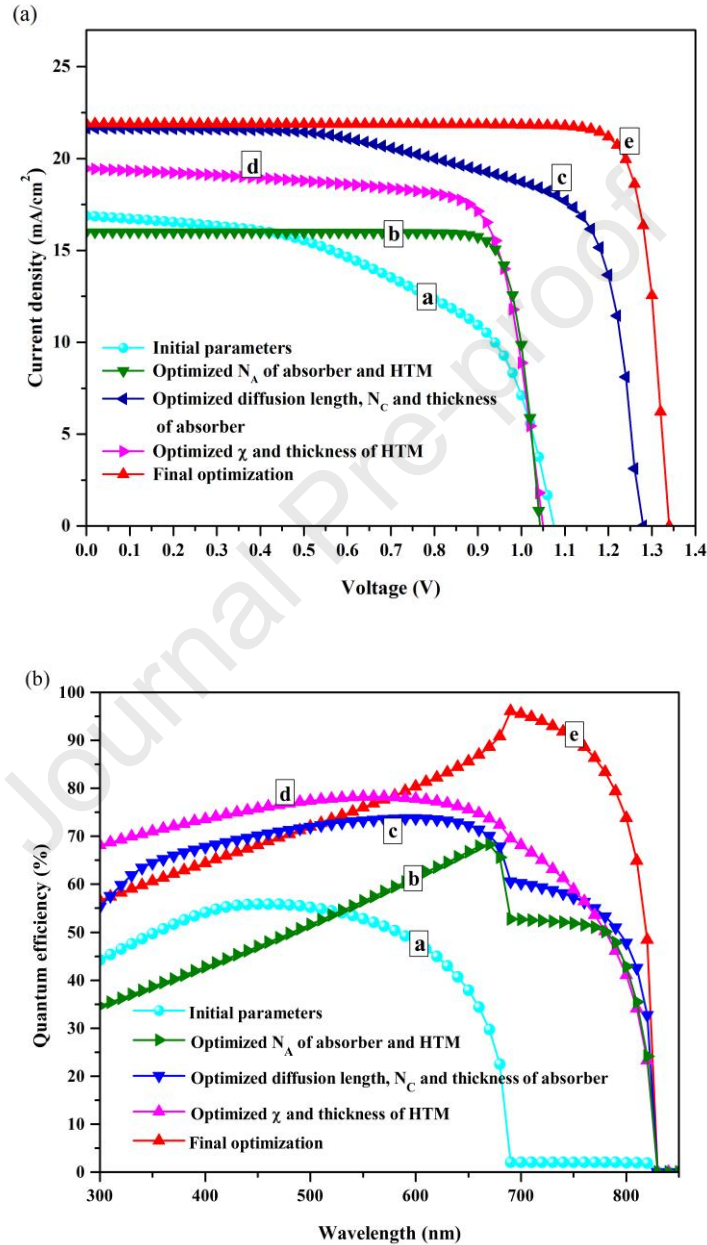


Fig. 4. Simulated (a) optimized J-V curves and (b) QE curves of CZTS based inverted PSC

Input parameters are validated by the consistent performance of simulated and real device. From Fig. 4b, red shifting of optical absorption edge is occurred at 690 nm while traversing entire visible spectrum having peak absorbance at 450 nm.

4.1 Influence of N_A of absorber and HTM

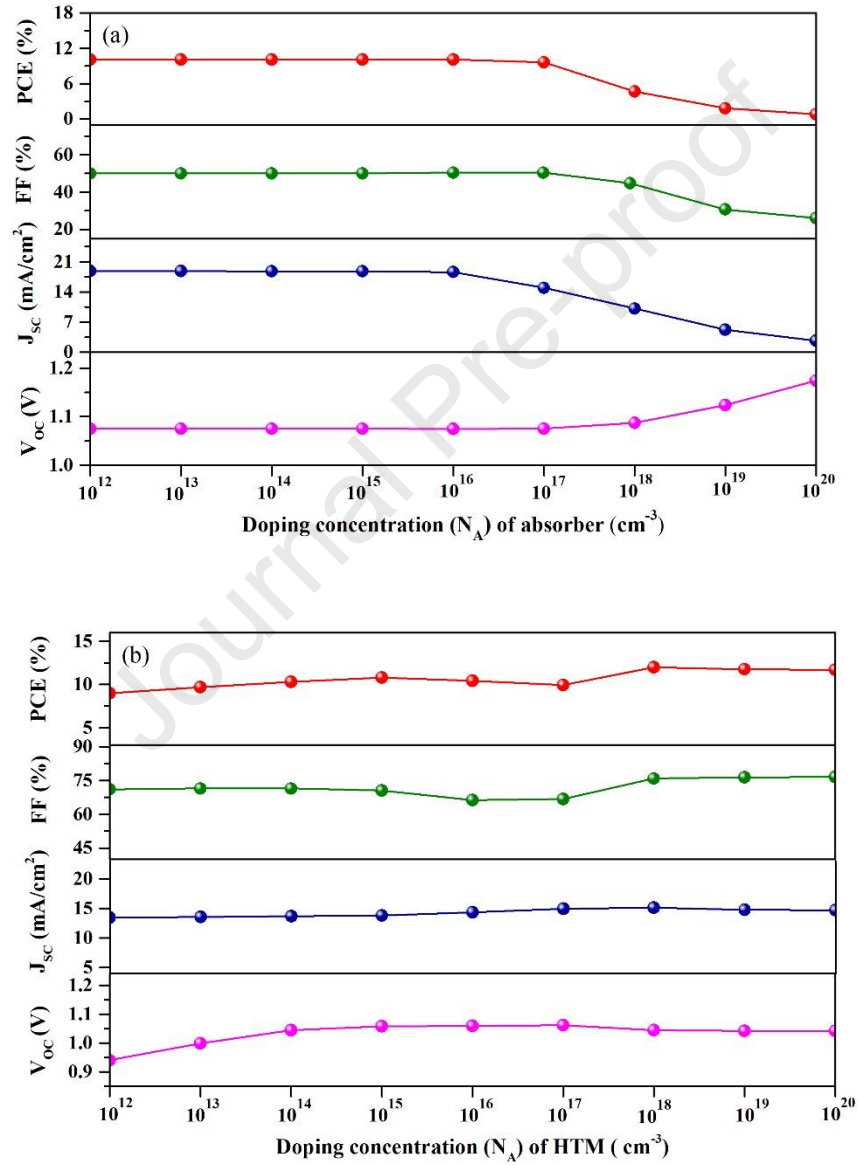


Fig. 5. Variation in performance parameters of CZTS based inverted PSC with N_A of (a) absorber (b) CZTS

Absorber layer has significant role in light absorption and charge collection at the electrodes. Doping is important process to improve the efficiency of inverted PSCs. For n-type or p-type doping in absorber layer, self-doping technique can be used. $\text{CH}_3\text{NH}_3\text{PbI}_3$ is synthesized from lead iodide (PbI_2) and methyl ammonium iodide (MAI) and ratio between PbI_2 and MAI can control the type of intrinsic defect and doping in the absorber. After thermal annealing, excess and deficit of PbI_2 in absorber layer is n-doped and p-doped respectively. Variation in the performance of inverted PSC with different N_A of absorber is shown in Fig. 5a. It is observed that PCE maintains constant when N_A of absorber is less than $1 \times 10^{17} \text{ cm}^{-3}$ followed by a decrease in PCE after N_A is higher than $1 \times 10^{17} \text{ cm}^{-3}$. J_{sc} also demonstrates the similar behaviour with a turning point at N_A of $1 \times 10^{16} \text{ cm}^{-3}$. When N_A of absorber is small, transport and collection of charge carriers become more efficient as indicated from the above results. Therefore, control of N_A of the absorber is very important to improve the performance of inverted PSCs. It is also noted that J_{sc} decreases when N_A is beyond $1 \times 10^{16} \text{ cm}^{-3}$. The built-in electric field increases with increasing N_A which effectively influence the performance of inverted PSCs. Auger recombination is the main cause of decrease in J_{sc} with increasing N_A of the absorber. When N_A of absorber increases beyond $1 \times 10^{16} \text{ cm}^{-3}$, Auger recombination rate also increases which deteriorates the performance of the device. Proper choice of N_A of absorber increases both the J_{sc} and V_{oc} , which in turn enhances the PCE. While too high N_A in the absorber degrades the performance of the device due to high charge recombination and high charge scattering. N_A of CZTS is also very critical for energy band alignment and charge recombination processes at the HTM/perovskite interface of the inverted PSC. The doping is mainly responsible for the enhancement of charge density and charge mobility in HTM which in turn improves electric conductivity and the performance of the device [52]. Immobile acceptor ions are generated by heavy doping level with deep coulomb trap and

small μ_p [53].

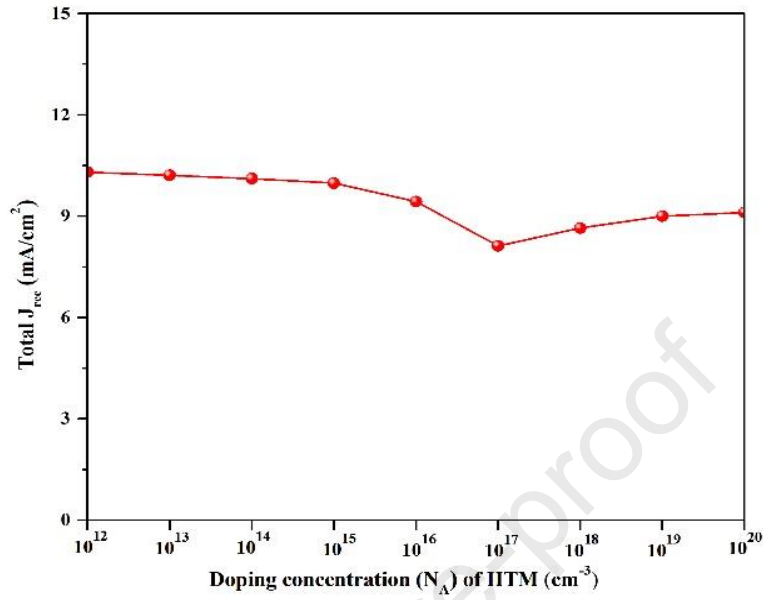


Fig. 6. Variation in total recombination current with N_A of CZTS

As shown in Fig 5b, J_{sc} of the device first stays constant when N_A of CZTS is smaller than $1 \times 10^{16} \text{ cm}^{-3}$, and then moderately increases to the maximum value with the increase of N_A of CZTS approaching $1 \times 10^{18} \text{ cm}^{-3}$, followed by a slight decrease when N_A is beyond $1 \times 10^{18} \text{ cm}^{-3}$. Furthermore, V_{oc} of the device first increases with the increase of N_A of CZTS then shows saturated behaviour when N_A of CZTS is between $1 \times 10^{16} \text{ cm}^{-3}$ to $1 \times 10^{20} \text{ cm}^{-3}$ as shown in Fig. 5b. FF is observed to decrease slowly with the increasing of N_A of CZTS up to $1 \times 10^{17} \text{ cm}^{-3}$, then increases up to $1 \times 10^{18} \text{ cm}^{-3}$ and stays saturate when N_A of CZTS is beyond $1 \times 10^{18} \text{ cm}^{-3}$. Similarly, PCE also exhibits the similar trend as FF with increasing N_A of CZTS as shown in Fig. 5b. Total recombination current sharply decreases when N_A increases from $1 \times 10^{15} \text{ cm}^{-3}$ to $1 \times 10^{17} \text{ cm}^{-3}$ as exhibited in Fig. 6, which could lead to an increase in J_{sc} of the device. On another aspect, when N_A of CZTS increases, the number of ionized acceptor ions and trap states increases which could cause a decrease of I_{sc} . The result of the combination of the two effects leads to a

minor increase of J_{sc} with different N_A of CZTS. For the similar reason, V_{oc} of the device increases with the increase of N_A of CZTS and saturate value of V_{oc} is obtained at 1.04 V as exhibited in Fig. 5b. In summary, it is concluded that N_A of absorber and HTM has optimized value of $1 \times 10^{15} \text{ cm}^{-3}$ and $1 \times 10^{18} \text{ cm}^{-3}$ respectively. The optimal performance with V_{oc} of 1.04 V, FF of 85.56 %, J_{sc} of 15.99 mA/cm^2 and PCE of 14.27 % is obtained when N_A of the absorber is $1 \times 10^{15} \text{ cm}^{-3}$. Fig. 4 shows the optimized J-V and QE characteristics in curve (b).

4.2 Influence of diffusion length, density of states (N_t) and thickness of absorber

Diffusion length is a crucial parameter which can be expressed in terms of N_t and need to be discussed in order to analyse the performance of inverted PSCs. The performance of inverted PSCs is significantly affected by the morphology and quality of the absorber layer. If the quality of the absorber film is not good, then diffusion length decreases and recombination rate of carriers becomes dominant in the absorber layer, which determines the V_{oc} of inverted PSC. Diffusion length is the average distance, charge carriers travel before recombination. Shockley-Read-Hall (SRH) recombination is the major phenomenon in order to calculate the recombination rate of charge carriers [54]. Furthermore, diffusion lengths of electrons and holes (L_n , L_p) are calculated by using equations (1) - (3). The initial value of diffusion length in the absorber is set to be $11.4 \text{ }\mu\text{m}$. The decrease of diffusion length in absorber leads towards poor performance of the inverted PSC.

Carrier life time is represented by $\tau_{n,p}$

$$\tau_{n,p} = \frac{1}{\sigma_{n,p} v_{th} N_t} \quad (1)$$

$\sigma_{n,p}$ is capture cross-section of the electrons and holes and $v_{th} = 10^7 \text{ cm/s}$ is the thermal velocity.

Diffusion coefficient (D) is given by

$$D = \frac{\mu k_B T}{q} \quad (2)$$

μ is the carrier mobility, k_B is Boltzmann constant, T is temperature in kelvin and q is magnitude of charge.

Diffusion length (L) is given by

$$L = \sqrt{D\tau} \quad (3)$$

The J-V and QE curves at different values of diffusion length are shown in Fig. 7. Based on the results, 360 μm is chosen as the optimized value of diffusion length of the perovskite absorber. Furthermore, carrier diffusion length can be used to analyse the effects of N_t on the performance

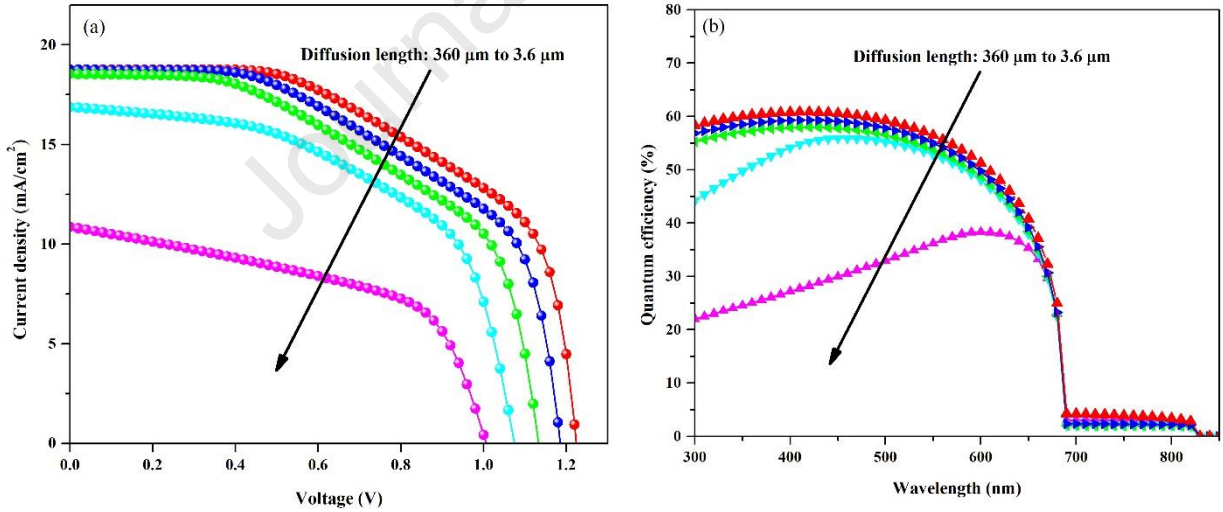
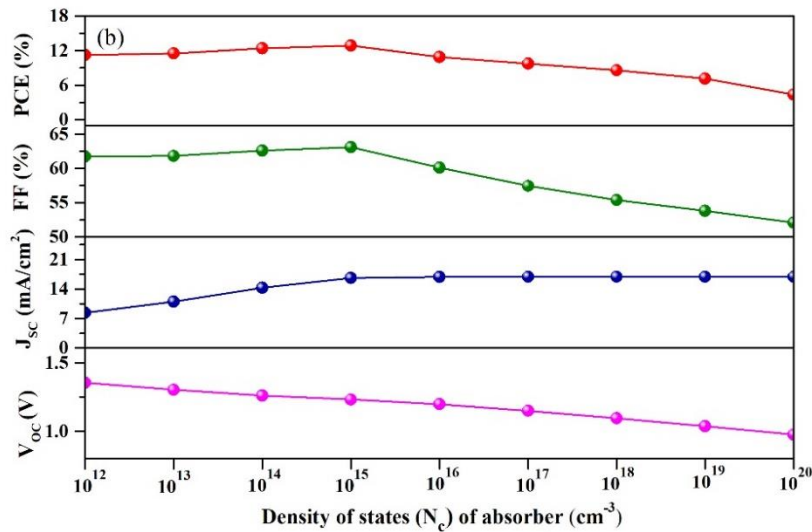
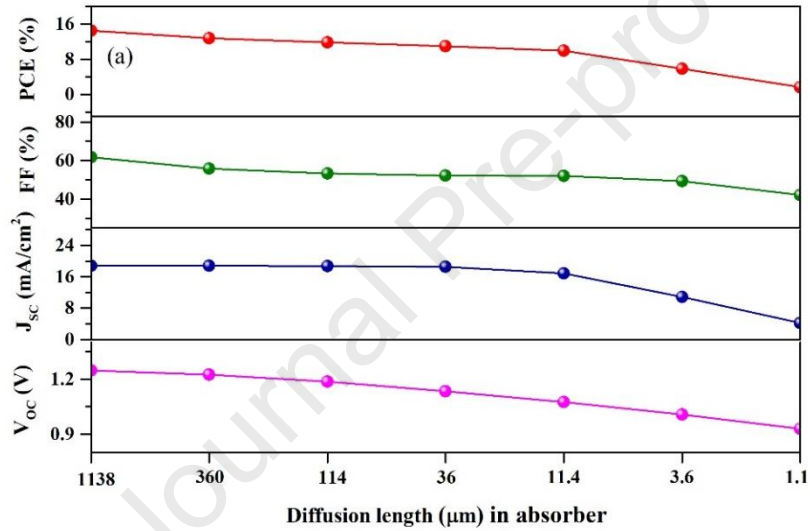


Fig. 7. Simulated (a) J-V curves (b) QE curve of CZTS based inverted PSC with varying diffusion length of the absorber

of devices dominated by SRH recombination. Diffusion length of absorber strongly affects FF being crucial parameter for the performance of PSCs shown in Fig 8a. For diffusion length larger than 114 μm , V_{oc} and J_{sc} saturate to 1.20 V and 18.75 mA/cm^2 respectively. Further, N_c in the absorber is also a critical parameter influencing the performance of p-i-n type PSCs. Effect of N_c of absorber is studied on the performance of p-i-n type PSC with CZTS as HTM. Fig. 8b shows the impact of N_c in the absorber on the performance of the perovskite device when N_c is changed from $1 \times 10^{12} \text{cm}^{-3}$ to $1 \times 10^{20} \text{cm}^{-3}$.



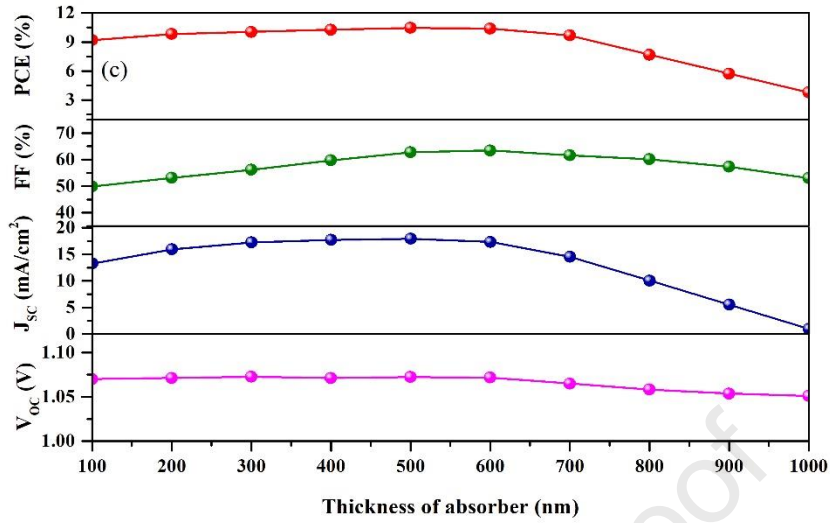


Fig. 8. Variation in performance parameters of CZTS based inverted PSC with (a) diffusion length (b) density of states (N_c) (c) thickness of absorber

PCE reaches the maximum value when N_c is $1 \times 10^{15} \text{ cm}^{-3}$ and decreases sharply when N_c exceeds $1 \times 10^{15} \text{ cm}^{-3}$. As number of electrons in absorber layer increases then reverse saturation current also increases. Therefore, V_{oc} decreases which leads towards lowering of PCE. Thickness of absorber is also an important parameter which has impact on the performance of p-i-n PSCs. Fig 8c demonstrates the variation of performance parameters with thickness of absorber. When thickness of the absorber is too small then J_{sc} and PCE are low owing to poor absorption of light in thin absorber layer. As thickness of absorber layer increases, J_{sc} and PCE increases owing to the fact that more charge carriers are generated due to higher light absorption in the thick absorber layer. The value of J_{sc} and PCE attains the maximum when thickness of the absorber is between 500 nm to 600 nm. The performance of the device begins to decrease when the thickness of the absorber is above 600 nm due to poor charge carrier collection at respective electrodes due to higher recombination rates in much thicker layer of absorber. In previous device modelling of n-i-p type PSCs, 600 nm thickness was also used to optimize the PCE of device as much as 21.32 % [6]. The optimum performance with V_{oc} of 1.27 V, FF of 70.86 %, J_{sc} of 21.65 mA/cm²

and PCE of 19.48 % is obtained under diffusion length of 360 μm , N_c of $1 \times 10^{15} \text{ cm}^{-3}$ and thickness of 600 nm of absorber layer. The optimized J-V and QE characteristics are shown in curve (c) of Fig 4.

4.3 Influence of χ and thickness of HTM

Band offset at HTM / absorber interface is significant parameter for the performance of solar cells. It affects carrier recombination rate at interface and the resulted V_{oc} of the device. The band offset can be modified by varying the values of χ of CZTS from 3.9 eV to 4.4 eV. Influence of different χ values of CZTS on the band offset at the HTM / absorber interface is shown in Fig. 9. Energy spikes are formed at the HTM/absorber interface, and the size of the spike increases with the increase of χ value of CZTS, which caused by an increased electric field across the interface. Diffusion of holes from HTM to absorber is affected by the energy level of holes in HTM, while high χ offers hindrance in the hole diffusion process, which leads to the lower charge carrier collection and higher charge carrier recombination thus results in poor FF and low device performance. Fig. 9b exhibits the variation in the device performance parameters with χ of CZTS. The χ value of 3.9 eV - 4.0 eV yields better performance of device. When χ of CZTS is high (more than 4.0 eV), PCE and FF decreases appreciably accompanied by J_{sc} decreases sharply after 4.0 eV. Furthermore, the thickness of CZTS also has crucial role in the performance of device because charge generation, transport, and recombination rate are all affected by the variation in thickness of CZTS.

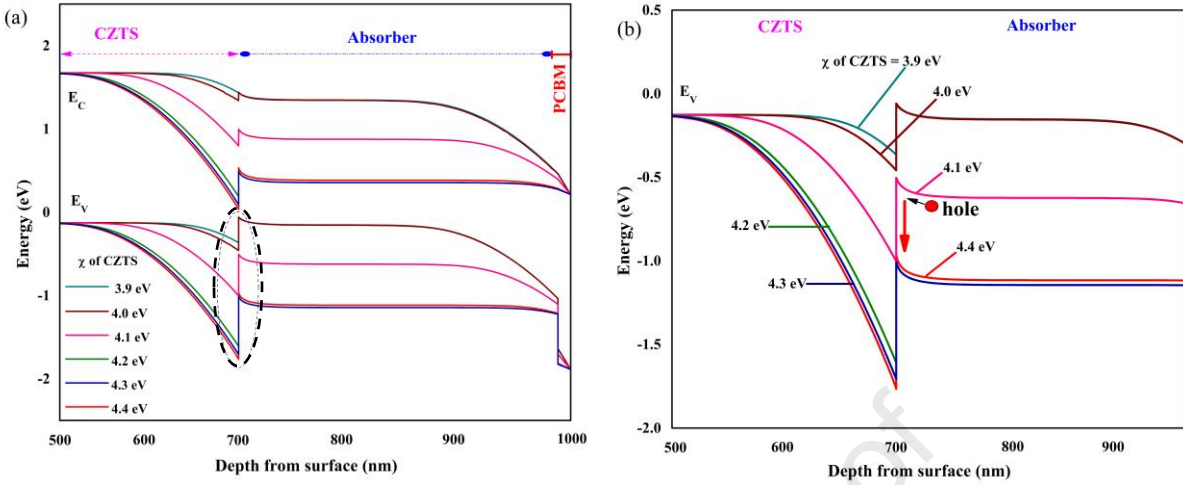


Fig. 9. Variation in the energy bands at HTM/absorber interface of inverted PSC with different values of χ of CZTS (a) total device (b) close up at HTM/absorber interface

Table 3.

Optimized parameters of the inverted PSC with CZTS as HTM

Optimized parameters	Absorber ($\text{CH}_3\text{NH}_3\text{PbI}_3$)	HTM (CZTS)
Doping density (cm^{-3})	1×10^{15}	1×10^{18}
Electron affinity (eV)	-	4
Diffusion length (μm)	360	-
Thickness (nm)	600	100
Density of states (cm^{-3})	1×10^{15}	-

It is shown in Fig. 10a that J_{sc} decreases sharply when thickness of CZTS increases from 120 nm to 500 nm, followed by a slow decrease when the thickness is beyond 500 nm. V_{oc} shows very small change with the increasing thickness of CZTS, which is influenced by the resistivity changes with the increasing thickness of CZTS. The best FF of 66 % is obtained when thickness of CZTS is ~100 nm and poor FF is 45 % is obtained when thickness is 900 nm. PCE of the device exhibits

the same trend as FF as shown in Fig. 10a.

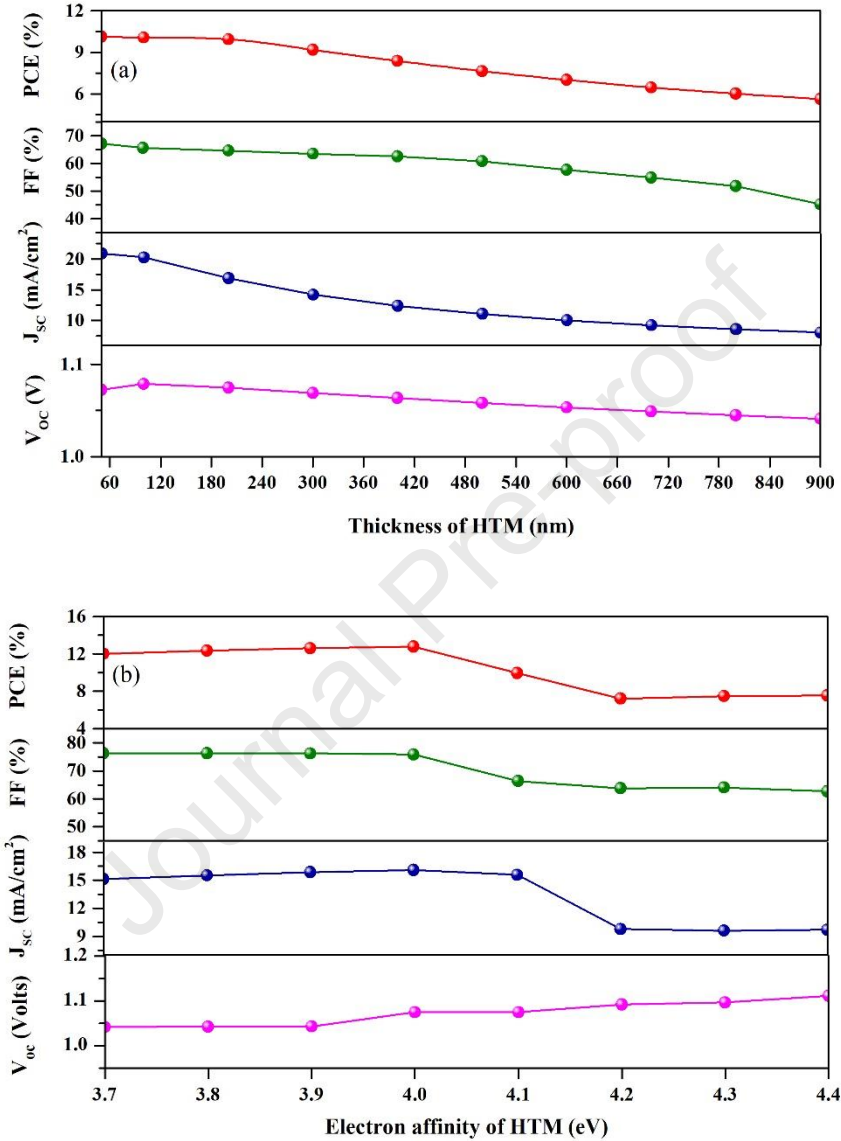


Fig. 10. Variation in performance parameters of CZTS based inverted PSC with (a) thickness of CZTS (b) χ of CZTS

Optimum performance with J_{sc} of 19.44 mA/cm², PCE of 15.42 %, FF of 75.52 % and V_{oc} of 1.04 V is obtained under the optimized χ of 4.0 eV and CZTS thickness of 100 nm (0.1 μ m). The optimized J-V and QE characteristics are shown in curve (d) in Fig. 4.

Table 4

Comparison between various nip and pin PSCs with CZTS as HTM

Nature of work	Architecture of device	Performance parameters			
		V_{oc} (volts)	J_{sc} (mA/cm ²)	FF (%)	PCE (%)
Experimental [55]	n-i-p	0.830	18.2	68	10.27
Experimental [56]	n-i-p	0.940	7.36	70.01	4.84
Experimental [57]	n-i-p	1.06	20.54	58.7	12.75
Experimental [58]	p-i-n	0.82	9.70	76.10	6.02
Theoretical [37]	n-i-p	1.15	26.45	74.61	22.70
Theoretical [59]	n-i-p	1.057	22.76	84.17	20.25

Table 5

Device simulation and experimental results of photovoltaic parameters with CZTS based p-i-n PSCs using SCAPS

Parameters	Our Experimental results	Our device simulation results				
		Initial	Optimized N_A of absorber and HTM	Optimized χ and thickness of HTM	Optimized N_c , CB DOS and thickness of absorber	Final optimization
PCE (%)	9.72	9.95	14.27	15.42	19.48	25.43
FF (%)	53.24	54.85	85.56	75.52	70.86	87.12
J_{sc} (mA/cm ²)	15.63	16.88	15.99	19.44	21.65	21.89
V_{oc} (V)	1.03	1.07	1.04	1.05	1.27	1.33

Table 4 shows the comparison between n-i-p and p-i-n PSCs with CZTS as HTM. It is clear that n-i-p PSCs have attained PCE of 12.75 % experimentally while PCE of 22.70 % theoretically. But p-i-n PSCs only attained PCE of 6.02 % experimentally while no device simulation was found in literature for p-i-n PSCs with CZTS as HTM. In this research work, encouraging results, V_{oc} of

1.33 V, FF of 87.12 %, J_{sc} of 21.89 mA/cm² and PCE of 25.43 %, are achieved for p-i-n PSC with all optimized parameters listed in Table 3. The optimized physical parameters and corresponding performance parameters are shown in Table 5 while final optimized J-V and QE characteristics are depicted in curve (e) of Fig. 4. The enhanced performance of the device can be accomplished by improving both the absorber and CZTS layer's film morphology and crystalline quality. Doping of absorber and CZTS by other element could further enhance the interface and performance of the device.

5. Conclusion

In this work, CZTS has been investigated as HTM in planar p-i-n PSC. Device with the structure of FTO/CZTS/perovskite/PCBM/Ag showed PCE of 9.72 % with J_{sc} of 15.63 mA/cm², FF of 53.24 % and V_{oc} of 1.03 V. In order to optimize the device performance, various factors affecting the device performance were investigated theoretically to get maximum performance with this device structure. These factors include doping density of CZTS and MAPbI₃, electron affinity and thickness of CZTS, as well as the diffusion length of charge carriers, density of states and thickness of the absorber. Based on the simulation results of the device, the optimized device showed PCE as high as 25.43 % with J_{sc} of 21.89 mA/cm², FF of 87.12 % and V_{oc} of 1.33 V. For CZTS HTM layer, the optimized doping density, electron affinity and thickness is 1×10^{18} cm⁻³, 4 eV and 100 nm respectively. For perovskite absorber layer, the optimized parameters including doping density of 1×10^{15} cm⁻³, diffusion length of 360 μm, density of states of 1×10^{15} cm⁻³ and thickness of 600 nm. This research highlighted the working mechanism of p-i-n PSCs and analyzed the influence of key physical parameters on the performance of device. Furthermore, CZTS is highly hydrophobic which prevent moisture to reach the absorber. Therefore, it reduced charge recombination at HTM / perovskite interfaces and enhanced the stability of the device. It is concluded that use of CZTS as hole transport material is beneficial for stable, efficient and

cost-effective p-i-n PSCs. Our work provides important guidelines for designing of high performance p-i-n PSCs.

Acknowledgement

Authors acknowledge the funding from Higher Education Commission, Pakistan for National Research Programme for Universities (NRPU) [Project number 8545].

Conflict of Interest

The authors declare no conflict of interest.

References

- [1] Y. Chen, L. Zhang, Y. Zhang, H. Gao, H. Yan, Large-area perovskite solar cells-a review of recent progress and issues, *RSC Adv.* 8 (2018) 10489–10508. <https://doi.org/10.1039/c8ra00384j>.
- [2] Z. Shi, A. Jayatissa, Perovskites-Based Solar Cells: A Review of Recent Progress, *Materials and Processing Methods*, *Materials (Basel)*. 11 (2018) 729. <https://doi.org/10.3390/ma11050729>.
- [3] A.R. Jeyaraman, S.K. Balasingam, C. Lee, H. Lee, B. Balakrishnan, S. Manickam, M. Yi, H.J. Kim, K. Sivalingam Nallathambi, Y. Jun, H. Kuzhandaivel, Enhanced solar to electrical energy conversion of titania nanoparticles and nanotubes-based combined photoanodes for dye-sensitized solar cells, *Mater. Lett.* 243 (2019) 180–182. <https://doi.org/10.1016/j.matlet.2019.02.006>.
- [4] H. Tang, S. He, C. Peng, A Short Progress Report on High-Efficiency Perovskite Solar Cells, *Nanoscale Res. Lett.* 12 (2017) 410. <https://doi.org/10.1186/s11671-017-2187-5>.

- [5] A. Kojima, K. Teshima, Y. Shirai, T. Miyasaka, Organometal Halide Perovskites as Visible-Light Sensitizers for Photovoltaic Cells, *J. Am. Chem. Soc.* 131 (2009) 6050–6051. <https://doi.org/10.1021/ja809598r>.
- [6] S.Z. Haider, H. Anwar, M. Wang, A comprehensive device modelling of perovskite solar cell with inorganic copper iodide as hole transport material, *Semicond. Sci. Technol.* 33 (2018) 1–12. <https://doi.org/10.1088/1361-6641/aaa596>.
- [7] S.Z. Haider, H. Anwar, Y. Jamil, M. Shahid, A comparative study of interface engineering with different hole transport materials for high-performance perovskite solar cells, *J. Phys. Chem. Solids.* 136 (2020) 1–11. <https://doi.org/10.1016/j.jpcs.2019.109147>.
- [8] S.Z. Haider, H. Anwar, M. Wang, Theoretical Device Engineering for High- Performance Perovskite Solar Cells Using CuSCN as Hole Transport Material Boost the Efficiency Above 25%, *Phys. Status Solidi.* 216 (2019) 1–12. <https://doi.org/10.1002/pssa.201900102>.
- [9] J. Burschka, N. Pellet, S.J. Moon, R. Humphry-Baker, P. Gao, M.K. Nazeeruddin, M. Grätzel, Sequential deposition as a route to high-performance perovskite-sensitized solar cells, *Nature.* 499 (2013) 316–319. <https://doi.org/10.1038/nature12340>.
- [10] Y.J. Jeon, S. Lee, R. Kang, J.E. Kim, J.S. Yeo, S.H. Lee, S.S. Kim, J.M. Yun, D.Y. Kim, Planar heterojunction perovskite solar cells with superior reproducibility, *Sci. Rep.* 4 (2014). <https://doi.org/10.1038/srep06953>.
- [11] K.C. Wang, J.Y. Jeng, P.S. Shen, Y.C. Chang, E.W.G. Diau, C.H. Tsai, T.Y. Chao, H.C. Hsu, P.Y. Lin, P. Chen, T.F. Guo, T.C. Wen, P-type mesoscopic nickel oxide/organometallic perovskite heterojunction solar cells, *Sci. Rep.* 4 (2014). <https://doi.org/10.1038/srep04756>.

- [12] H.S. Jung, N.-G. Park, Perovskite Solar Cells: From Materials to Devices, *Small*. 11 (2015) 10–25. <https://doi.org/10.1002/sml.201402767>.
- [13] E. Bi, W. Tang, H. Chen, Y. Wang, J. Barbaud, T. Wu, W. Kong, P. Tu, H. Zhu, X. Zeng, J. He, S. ichi Kan, X. Yang, M. Grätzel, L. Han, Efficient Perovskite Solar Cell Modules with High Stability Enabled by Iodide Diffusion Barriers, *Joule*. 3 (2019) 2748–2760. <https://doi.org/10.1016/j.joule.2019.07.030>.
- [14] D. Zhou, T. Zhou, Y. Tian, X. Zhu, Y. Tu, Perovskite-Based Solar Cells: Materials, Methods, and Future Perspectives, *J. Nanomater.* 2018 (2018). <https://doi.org/10.1155/2018/8148072>.
- [15] P. Cui, D. Wei, J. Ji, H. Huang, E. Jia, S. Dou, T. Wang, W. Wang, M. Li, Planar p–n homojunction perovskite solar cells with efficiency exceeding 21.3%, *Nat. Energy*. 4 (2019) 150–159. <https://doi.org/10.1038/s41560-018-0324-8>.
- [16] L.-B. Chang, C.-C. Tseng, G. Wu, W.-S. Feng, M.-J. Jeng, L.-C. Chen, K.-L. Lee, E. Popko, L. Jacak, K. Gwozdz, L.-B. Chang, C.-C. Tseng, G. Wu, W.-S. Feng, M.-J. Jeng, L.-C. Chen, K.-L. Lee, E. Popko, L. Jacak, K. Gwozdz, Low-Cost $\text{CuIn}_{1-x}\text{Ga}_x\text{Se}_2$ Ultra-Thin Hole-Transporting Material Layer for Perovskite/CIGSe Heterojunction Solar Cells, *Appl. Sci.* 9 (2019) 719. <https://doi.org/10.3390/app9040719>.
- [17] V. Trifiletti, N. Manfredi, A. Listorti, D. Altamura, C. Giannini, S. Colella, G. Gigli, A. Rizzo, Engineering TiO_2 /Perovskite Planar Heterojunction for Hysteresis-Less Solar Cells, *Adv. Mater. Interfaces*. 3 (2016) 1600493. <https://doi.org/10.1002/admi.201600493>.
- [18] E. Li, W. Li, L. Li, H. Zhang, C. Shen, Z. Wu, W. Zhang, X. Xu, H. Tian, W.H. Zhu, Y. Wu, Efficient p-i-n structured perovskite solar cells employing low-cost and highly

- reproducible oligomers as hole transporting materials, *Sci. China Chem.* 62 (2019) 767–774. <https://doi.org/10.1007/s11426-018-9452-9>.
- [19] Y. Zhang, X. Hu, L. Chen, Z. Huang, Q. Fu, Y. Liu, L. Zhang, Y. Chen, Flexible, hole transporting layer-free and stable $\text{CH}_3\text{NH}_3\text{PbI}_3$ / PC61BM planar heterojunction perovskite solar cells, *Org. Electron.* 30 (2016) 281–288. <https://doi.org/10.1016/J.ORGEL.2016.01.002>.
- [20] J.-Y. Jeng, Y.-F. Chiang, M.-H. Lee, S.-R. Peng, T.-F. Guo, P. Chen, T.-C. Wen, $\text{CH}_3\text{NH}_3\text{PbI}_3$ Perovskite/Fullerene Planar-Heterojunction Hybrid Solar Cells, *Adv. Mater.* 25 (2013) 3727–3732. <https://doi.org/10.1002/adma.201301327>.
- [21] J.H. Heo, H.J. Han, D. Kim, T.K. Ahn, S.H. Im, Hysteresis-less inverted $\text{CH}_3\text{NH}_3\text{PbI}_3$ planar perovskite hybrid solar cells with 18.1% power conversion efficiency, *Energy Environ. Sci.* 8 (2015) 1602–1608. <https://doi.org/10.1039/C5EE00120J>.
- [22] W.-Y. Chen, L.-L. Deng, S.-M. Dai, X. Wang, C.-B. Tian, X.-X. Zhan, S.-Y. Xie, R.-B. Huang, L.-S. Zheng, Low-cost solution-processed copper iodide as an alternative to PEDOT:PSS hole transport layer for efficient and stable inverted planar heterojunction perovskite solar cells, *J. Mater. Chem. A.* 3 (2015) 19353–19359. <https://doi.org/10.1039/C5TA05286F>.
- [23] T.R. Chou, S.H. Chen, Y. Te Chiang, T.T. Chang, C.W. Lin, C.Y. Chao, Highly conductive PEDOT:PSS film by doping p-toluenesulfonic acid and post-treatment with dimethyl sulfoxide for ITO-free polymer dispersed liquid crystal device, *Org. Electron.* 48 (2017) 223–229. <https://doi.org/10.1016/j.orgel.2017.05.052>.
- [24] W.H. Chen, L. Qiu, P. Zhang, P.C. Jiang, P. Du, L. Song, J. Xiong, F. Ko, Simple fabrication

- of a highly conductive and passivated PEDOT:PSS film: Via cryo-controlled quasi-congealing spin-coating for flexible perovskite solar cells, *J. Mater. Chem. C*. 7 (2019) 10247–10256. <https://doi.org/10.1039/c9tc02744k>.
- [25] S.K. Hau, H.L. Yip, N.S. Baek, J. Zou, K. O'Malley, A.K.Y. Jen, Air-stable inverted flexible polymer solar cells using zinc oxide nanoparticles as an electron selective layer, *Appl. Phys. Lett.* 92 (2008). <https://doi.org/10.1063/1.2945281>.
- [26] L. Qian, Y. Zheng, J. Xue, P.H. Holloway, Stable and efficient quantum-dot light-emitting diodes based on solution-processed multilayer structures, *Nat. Photonics*. 5 (2011) 543–548. <https://doi.org/10.1038/nphoton.2011.171>.
- [27] W. Wang, H. Shen, L.H. Wong, Z. Su, H. Yao, Y. Li, A 4.92% efficiency $\text{Cu}_2\text{ZnSnS}_4$ solar cell from nanoparticle ink and molecular solution, *RSC Adv.* 6 (2016) 54049–54053. <https://doi.org/10.1039/c6ra08604g>.
- [28] L.C. Chen, J.C. Chen, C.C. Chen, C.G. Wu, Fabrication and Properties of High-Efficiency Perovskite/PCBM Organic Solar Cells, *Nanoscale Res. Lett.* 10 (2015). <https://doi.org/10.1186/s11671-015-1020-2>.
- [29] U. Syafiq, N. Ataollahi, R. DiMaggio, P. Scardi, Solution-based synthesis and characterization of $\text{Cu}_2\text{ZnSnS}_4$ (CZTS) thin films, *Molecules*. 24 (2019). <https://doi.org/10.3390/molecules24193454>.
- [30] P.R. Ghediya, T.K. Chaudhuri, Dark and photo-conductivity of doctor-bladed CZTS films above room temperature, *J. Phys. D: Appl. Phys.* 48 (2015). <https://doi.org/10.1088/0022-3727/48/45/455109>.

- [31] A. El Karkri, Z. El Malki, M. Bouachrine, F. Serein-Spirau, J.M. Sotiropoulos, Characterization and simulation study of organic solar cells based on donor-acceptor (D-p-A) molecular materials, *RSC Adv.* 10 (2020) 18816–18823. <https://doi.org/10.1039/d0ra01815e>.
- [32] H. Abedini-Ahangarkola, S. Soleimani-Amiri, Design and analysis of high efficiency perovskite solar cells with light trapping nano-textured substrates, *Int. J. Eng. Trans. A Basics.* 34 (2021) 873–880. <https://doi.org/10.5829/ije.2021.34.04a.13>.
- [33] M. Mehrabian, S. Dalir, 11.73% efficient perovskite heterojunction solar cell simulated by SILVACO ATLAS software, *Optik (Stuttg.)* 139 (2017) 44–47. <https://doi.org/10.1016/j.ijleo.2017.03.077>.
- [34] X. Yu, X. Zou, J. Cheng, C. Chang, Z. Zhou, G. Li, B. Liu, J. Wang, D. Chen, Y. Yao, Numerical simulation analysis of effect of energy band alignment and functional layer thickness on the performance for perovskite solar cells with $\text{Cd}_{1-x}\text{Zn}_x\text{S}$ electron transport layer, *Mater. Res. Express.* 7 (2020). <https://doi.org/10.1088/2053-1591/abbf12>.
- [35] S. Karthick, S. Velumani, J. Bouclé, Experimental and SCAPS simulated formamidinium perovskite solar cells: A comparison of device performance, *Sol. Energy.* 205 (2020) 349–357. <https://doi.org/10.1016/j.solener.2020.05.041>.
- [36] P.K. Patel, Device simulation of highly efficient eco-friendly $\text{CH}_3\text{NH}_3\text{SnI}_3$ perovskite solar cell, *Sci. Rep.* 11 (2021) 3082. <https://doi.org/10.1038/s41598-021-82817-w>.
- [37] I. Kabir, S.A. Mahmood, Analysis of highly efficient perovskite solar cells with inorganic hole transport material, *Chinese Phys. B.* 28 (2019) 1–7. <https://doi.org/10.1088/1674-1056/ab520f>.

- [38] M.D. Wanda, S. Ouédraogo, F. Tchoffo, F. Zougmore, J.M.B. Ndjaka, Numerical Investigations and Analysis of $\text{Cu}_2\text{ZnSnS}_4$ Based Solar Cells by SCAPS-1D, *Int. J. Photoenergy*. 2016 (2016) 1–9. <https://doi.org/10.1155/2016/2152018>.
- [39] J. Jeng, Y. Chiang, M. Lee, T. Guo, P. Chen, T. Wen, Methylammonium lead iodide perovskite/fullerene-based hybrid solar cells, *SPIE Newsroom*. (2013) 3–6. <https://doi.org/10.1117/2.1201307.005033>.
- [40] B.W. Larson, J.B. Whitaker, X. Bin Wang, A.A. Popov, G. Rumbles, N. Kopidakis, S.H. Strauss, O. V. Boltalina, Electron affinity of Phenyl-C61-butyric acid methyl ester (PCBM), *J. Phys. Chem. C*. 117 (2013) 14958–14964. <https://doi.org/10.1021/jp403312g>.
- [41] R. Lydia, P. Sreedhara Reddy, Effect of pH on the Characteristics of $\text{Cu}_2\text{ZnSnS}_4$ Nanoparticles, *ISRN Condens. Matter Phys.* 2013 (2013) 1–5. <https://doi.org/10.1155/2013/145205>.
- [42] L. Calió, S. Kazim, M. Grätzel, S. Ahmad, Hole-Transport Materials for Perovskite Solar Cells, *Angew. Chemie - Int. Ed.* 55 (2016) 14522–14545. <https://doi.org/10.1002/anie.201601757>.
- [43] Y.A.M. Ismail, T. Soga, T. Jimbo, Effect of Composition on Conjugation Structure and Energy Gap of P3HT : PCBM Organic Solar Cell, *Int. J. New Horizons Phys.* 93 (2015) 87–93.
- [44] A. Crovetto, M.K. Huss-Hansen, O. Hansen, How the relative permittivity of solar cell materials influences solar cell performance, *Sol. Energy*. 149 (2017) 145–150. <https://doi.org/10.1016/j.solener.2017.04.018>.

- [45] A. Yang, Investigation of Optical and Dielectric Constants of Organic-Inorganic $\text{CH}_3\text{NH}_3\text{PbI}_3$ Perovskite Thin Films, *J Nanomed Nanotechnol.* 7 (2016) 407. <https://doi.org/10.4172/2157-7439.1000407>.
- [46] S. Torabi, F. Jahani, I. Van Severen, C. Kanimozhi, S. Patil, R.W.A. Havenith, R.C. Chiechi, L. Lutsen, D.J.M. Vanderzande, T.J. Cleij, J.C. Hummelen, L.J.A. Koster, Strategy for enhancing the dielectric constant of organic semiconductors without sacrificing charge carrier mobility and solubility, *Adv. Funct. Mater.* 25 (2015) 150–157. <https://doi.org/10.1002/adfm.201402244>.
- [47] G. Giorgi, J.I. Fujisawa, H. Segawa, K. Yamashita, Small photocarrier effective masses featuring ambipolar transport in methylammonium lead iodide perovskite: A density functional analysis, *J. Phys. Chem. Lett.* 4 (2013) 4213–4216. <https://doi.org/10.1021/jz4023865>.
- [48] F.A. Jhuma, M.Z. Shaily, M.J. Rashid, Towards high-efficiency CZTS solar cell through buffer layer optimization, *Mater. Renew. Sustain. Energy.* 8 (2019) 1–7. <https://doi.org/10.1007/s40243-019-0144-1>.
- [49] C. Motta, F. El-Mellouhi, S. Sanvito, Charge carrier mobility in hybrid halide perovskites, *Sci. Rep.* 5 (2015) 12746. <https://doi.org/10.1038/srep12746>.
- [50] M. Jiang, X. Y, $\text{Cu}_2\text{ZnSnS}_4$ Thin Film Solar Cells: Present Status and Future Prospects, in: *Sol. Cells - Res. Appl. Perspect.*, InTech, 2013: pp. 107–143. <https://doi.org/10.5772/50702>.
- [51] G. Zuo, Z. Li, O. Andersson, H. Abdalla, E. Wang, M. Kemerink, Molecular Doping and Trap Filling in Organic Semiconductor Host-Guest Systems, *J. Phys. Chem. C.* 121 (2017) 7767–7775. <https://doi.org/10.1021/acs.jpcc.7b01758>.

- [52] S. Ameen, M.S. Akhtar, H.-S. Shin, M.K. Nazeeruddin, Charge-Transporting Materials for Perovskite Solar Cells, *Adv. Inorg. Chem.* 72 (2018) 185–246. <https://doi.org/10.1016/BS.ADIOCH.2018.05.009>.
- [53] S. Ohmagari, J. Pernot, E. Device, Learn more about Hole Mobility Doping and semiconductor characterizations SiGe Devices, (2018).
- [54] N. Anttu, Shockley–Queisser Detailed Balance Efficiency Limit for Nanowire Solar Cells, *ACS Photonics*. 2 (2015) 446–453. <https://doi.org/10.1021/ph5004835>.
- [55] S.B. Patel, A.H. Patel, J. V. Gohel, A novel and cost effective CZTS hole transport material applied in perovskite solar cells, *CrystEngComm*. 20 (2018) 7677–7687. <https://doi.org/10.1039/c8ce01337c>.
- [56] Z.J. Zhou, Y.Q. Deng, P.P. Zhang, D.X. Kou, W.H. Zhou, Y.N. Meng, S.J. Yuan, S.X. Wu, $\text{Cu}_2\text{ZnSnS}_4$ Quantum Dots as Hole Transport Material for Enhanced Charge Extraction and Stability in All-Inorganic CsPbBr_3 Perovskite Solar Cells, *Sol. RRL*. 3 (2019). <https://doi.org/10.1002/solr.201800354>.
- [57] Q. Wu, C. Xue, Y. Li, P. Zhou, W. Liu, J. Zhu, S. Dai, C. Zhu, S. Yang, Kesterite $\text{Cu}_2\text{ZnSnS}_4$ as a Low-Cost Inorganic Hole-Transporting Material for High-Efficiency Perovskite Solar Cells, *ACS Appl. Mater. Interfaces*. 7 (2015) 28466–28473. <https://doi.org/10.1021/acsami.5b09572>.
- [58] G.Y. Ashebir, C. Dong, Z. Wan, J. Qi, J. Chen, Q. Zhao, W. Chen, M. Wang, Solution-processed $\text{Cu}_2\text{ZnSnS}_4$ nanoparticle film as efficient hole transporting layer for stable perovskite solar cells, *J. Phys. Chem. Solids*. 129 (2019) 204–208. <https://doi.org/10.1016/j.jpcs.2019.01.008>.

- [59] N. Cheng, W. Li, S. Sun, Z. Zhao, Z. Xiao, Z. Sun, W. Zi, L. Fang, A simulation study of valence band offset engineering at the perovskite/Cu₂ZnSn(Se_{1-x}S_x)₄ interface for enhanced performance, *Mater. Sci. Semicond. Process.* 90 (2019) 59–64. <https://doi.org/10.1016/j.mssp.2018.10.006>.

Journal Pre-proof

Declaration of interests

The authors declare that they have no known competing financial interests or personal relationships that could have appeared to influence the work reported in this paper.

Journal Pre-proof